Continuous convex relaxation methodology applied to retroperitoneal tumors

C. Suárez-Mejías [1], J.A. Pérez-Carrasco [2], C. Serrano, [2] C. Parra Calderón [1], B. Acha [2]

[1] Technological Innovation Group, Virgen del Rocío University Hospital, Sevilla, Spain, {cristina.suarez.exts, carlos.parra.sspa}@juntadeandalucia.es

[2] Signal Theory and Communications Department, Sevilla, Spain, {jperez, bacha, cserrano}@us.es

Abstract

In this paper, two algorithms for the segmentation of tumors in soft tissues are presented and compared. These algorithms are applied to the segmentatiion of retroperitoneal tumors. Method: The algorithms are based on a continuous convex relaxation methodology with the introduction of an accumulated gradient distance (AGD). Algorithm 1 is based on two-label convex relaxation and Algorithm 2 applies multilabel convex relaxation. Results: Algorithms 1 and 2 are tested on a database of 6 CT volumes and their results are compared with the manual segmentation. The multilabel version performs better, achieving a 91% of sensitivity, 100% of specificity, 88% of PPV and 89% of Dice index. Conclusions: To the best of our knowledge, this is the first time that the segmentation of retroperitoneal tumors has been addressed. Two segmentation algorithms have been compared and the multilabel version obtains very good results.

Introduction

The segmentation of tumors in radiological images is a challenge. Methods based on active contour are widely used for tumors in liver [1], lung [2-4], prostate [5-7] and lymph nodes [8,9] in axillaries and pelvic regions. Besides, active curve evolution can lead to local optima of the minimization energy function and suffers from high sensitivity to initialization. Graph cut techniques have the advantage of guaranteeing global optima almost in real time. Thus, these techniques have been successfully applied in recent works [10][11]. In [12-16] the authors also applied graph-cut for the segmentation of lung, brain and prostate tumors. Also, Zhang et al. [17] used it for cervical lymph nodes on sonograms and Feulner et at [18, 19] for lymph node detection in the mediastinum. In this paper retroperitoneal masses are segmented. They are a diverse group of benign and malignant tumors that arise within the retroperitoneal space but outside the major organs in this space. Among the retroperitoneal masses, 70%–80% are malignant [20]. The retroperitoneal space is hidden toward the back of the abdomen where organs are quite mobile. Thus, retroperitoneal tumors do not have an established pattern and can grow quite large, even moving organs out of their path, before being discovered. Due to these characteristics, well-known methods for the automatic segmentation of tumors does not usually perform well when they are applied to segment this kind of tumors.

In this paper, two algorithms for segmentation of retroperitoneal tumors are proposed and compared. The proposed algorithms are based on continuous convex relaxation method [21-24] which shares the advantages of both active curves and graph cuts. Some recent studies [25] showed that, in 3D, convex relaxation approaches outperform graph cuts in terms of speed and accuracy. In [26] is used to segment the carotid in 3D MRI images, in [27] to extract myocardial scar tissue, in [28] to segment the femoral artery lumen and outer wall surfaces, in [29] for lateral ventricles in preterm neonates and in [30,31] to delineate 3D prostate. In these algorithms the accumulated gradient distance is introduced as novelty in the minimization of the energies. A preliminary version based on two labels was published in [32] and tested with only three CT images. A second algorithm has been developed, that is based on a multilabel convex relaxation.

Methods

In this paper, a comparison between two algorithms for the segmentation of retroperitoneal tumors using a continuous convex relaxation methodology has been carried out. The two algorithms consist of four stages: a pre-processing step, a second stage to compute the accumulated gradient distance image, a continuous convex relaxation stage and a final post-processing stage to improve the segmentation results. The first algorithm implements a two-label segmentation. The second one uses a multi-label strategy to implement the segmentation.

Preprocessing stage

This stage is common for the two algorithms and it implements a contrast enhancement operation. First, the tumor is manually segmented in one CT slice. The manual segmentation does not need to be performed on a specific slice, only on a slice where the tumor is included. Furthermore, this segmentation does not have to be very precise. The same manual segmentation was used for the two algorithms. This manual segmentation is employed to estimate the mean Hounsfield level inside the tumor. Then, an exponential law is applied to all the slices within the CT volumes (see Eq. 1). According to the parameters of this exponential law, values close to the mean inside the tumor will have an approximate linear mapping whereas those values far from the mean will be closely saturated to 0 or 1.

$$output = \frac{1}{1+e^{-ov/level}} \quad (1)$$

In Eq. (1) *ov* is the Hounsfield gray level of the original image and *level* is the average Hounsfield value inside the tumor in the slice manually segmented.

ISBN: 978-84-608-3354-3

Computation of the Accumulated Gradient Distance Volume stage

The second step that both algorithms share is the computation of the *accumulated gradient distance* for each CT volume. In this stage the gradient of the volume *GV* is first computed in the three directions *x*, *y* and *z*. Once the gradient has been obtained we proceed to compute the accumulated gradient distance volume (A*GDV*) or gradient distance from the manually segmented tumor in one slice to the rest of the volume. To do this, the *generalized distance function algorithm* (*GDF*) described in [33] is used.

Let $N^+(p)$ be the 13 neighbors in the 26-connected neighborhood of p which are scanned before p in a raster scan. Similarly, $N^-(p)$ are the 13 neighbors of p which are scanned before p in an antiraster scan. Let GV be the gradient volume computed in the previous step. And let $C_f(p,q) = GV(p) + GV(q)$ be the associated cost of two neighboring voxels p and q. The GDF algorithm proceeds as follows:

1) Initialize the accumulated gradient distance, d_f, of pixel p as: $d_f(p) = 0$, if p belongs to the tumor in the manually segmented slice and $d_f(p) = +\infty$ otherwise.

2) Iterate until stability, for each pixel *p*:

Scan image in raster order:

$$d_f \leftarrow \min\left\{d_f(p), \min\left\{d_f(q) + C_f(p,q), q \in N^+(p)\right\}\right\}. \quad (2)$$

Scan image in anti-raster order:

$$d_f \leftarrow \min\left\{d_f(p), \min\left\{d_f(q) + C_f(p,q), q \in N^-(p)\right\}\right\}. \quad (3)$$

The accumulated gradient distance provides low values in the tumor area and high values outside the tumor. Figure 1 illustrates the preprocessing and the information contained in the Gradient Distance Image.

(a) (b) (c)

Figure 1. *a) A slice of the patient before the enhancement operation, b) same slice after the contrast enhancement operation, c) Gradient Distance Image.*

Two-label Segmentation (Algorithm 1)

In this stage, the accumulated gradient distance image (AGDV) will be utilized to carry out the segmentation. In the two algorithms, the segmentation has been implemented using the fast continuous max-flow method (CMF) proposed by J. Yuan et al [21][23]. In the two-label implementation [32], the continuous convex relaxation algorithm solves the segmentation as the following minimization problem:

$$\min_{u(x)\in[0,1]} \int_\Omega (1-u(x))C_s(x)dx + \int_\Omega u(x)C_t(x)dx + \int_\Omega C(x)|\nabla u(x)|dx \quad (4)$$

Where C_s and C_t are regional terms, $u(x) \in [0,1]$ is the labeling function and $C(x)$ is a penalty function. The most right term of Eq. (4) is the regularization term and $|\nabla u(x)|$ is the absolute gradient of the labeling function $u(x)$, thus indicating the boundary of the segmented region.

If the minimization problem is well defined, the cost function $C_s(x)$ should take high values outside the tumor and low values inside the tumor. Similarly, $C_t(x)$ should take low values outside the tumor and high values inside the tumor.

In our implementation, the terms C_s and C_t are computed using the information provided by the *TAGD* as follows:

(5)

The constant 0.16 in Eq. (5) has been fixed experimentally. It corresponds to the average mean value of *AGDV* outside the tumor for the different cases that have been analyzed.

Multi-label Segmentation (Algorithm 2)

In Algorithm 2, the *AGD* 3D volume is thresholded in order to form a mask to be applied to the preprocessed image. The resultant 3D image after applying this mask to the preprocessed image is called *TAGD* (*Thresholded by Accumulated Gradient Distance*) image and it is used as input to the continuous convex relaxation segmentation

Differently to the two-label algorithm, in the multi-label segmentation algorithm the minimization function in Eq. (4) is substituted by:

$$\min_{u_i(x)\in[0,1]} \sum_{i=1}^{n} \int_\Omega (u_{i-1}(x) - u_i(x))\rho_i(x)dx + \int_\Omega C(x)|\nabla u_i(x)|dx \quad (6)$$

s.t. $1 = u_0(x) \geq u_1(x) \geq .. u_{n-1}(x) \geq u_n(x)$

where $u_i(x) \in [0,1]$ and the regional terms $\rho_i(x)$ must take low values within region I_i . As retroperitoneal tumors are usually composed by different ranges of gray levels, several labels are required to select them. Some experimental tests were done and the best option was to use four labels: one for the background, one for different tissues not belonging to the tumor , and two labels for the tumor. In this sense, $\rho_i(x)$ was defined as:

$$\begin{aligned} \rho_1(x) &= |TAGD(x) - 0| \\ \rho_2(x) &= |TAGD(x) - \mu + \sigma| \\ \rho_3(x) &= |TAGD(x) - \mu| \\ \rho_4(x) &= |TAGD(x) - \mu - 4\sigma| \end{aligned} \quad (7)$$

TAGD image is a 3D gray-level image where ideally, the tumor values are around μ, where μ is the average gray-level of the tumor and σ its standard deviation within the manually segmented slice. After the minimization, the tumor will be concentrated in the central labels, more

ISBN: 978-84-608-3354-3

specifically, in labels 2 and 3 and labels 1 and 4 will include background or other tissue values.

The penalty function in Eq. 6 is computed as follows:

$$C(x) = \frac{b}{1 + a \cdot \left| \nabla TAGD(x) \right|}, \; a,b > 0 \qquad (8)$$

where parameters *a* and *b* control the weight of the gradient in the penalty function $C(x)$ and $\left| \nabla TAGD(x) \right|$ is the absolute value of the gradient of the *TAGD* volume. The values for *a* and *b*, obtained experimentally, are 100 and 2 respectively.

Results

The algorithm 1 and the algorithm 2 have been programmed in MATLAB R2011a (The MathWorks Inc. 3 Apple Hill Drive. Natick, MA 01760-2098, US) and have been validated using 6 CT images of retroperitoneal tumors, each one composed by 200 512x512 slices. Some objective performance measurements have been calculated: Sensitivity (Se), Specificity (Sp), Positive Predictive Value (PPV), Jaccard index and Dice index. Both Jaccard and Dice coefficients measure the greement between two sets in terms of false positive, false negative, true negative and true positive counts. In our approach, true positives are those voxels classified as tumor both by the algorithm and the specialist. False positives are those voxels classified as tumor by the algorithm but not by the specialist. True negatives are voxels classified as not belonging to the tumor both by the tool and the specialist. Finally, false negatives are voxels classified as not belonging to the tumor by the algorithm but classified as tumor by the specialist. Table 1 shows these coefficients for the two algorithms in the 6 cases analyzed.

As shown in Table 1, Algorithm 1, which uses a two-label scheme, did not select tumors correctly in 2 out of the 6 cases analyzed, whereas Algorithm 2 (multilabel) selected properly the tumors in all the cases. In Fig. 1 comparisons between segmentation results obtained with Algorithm 1 and Algorithm 2 with respect to the manual segmentation (in red) are shown.

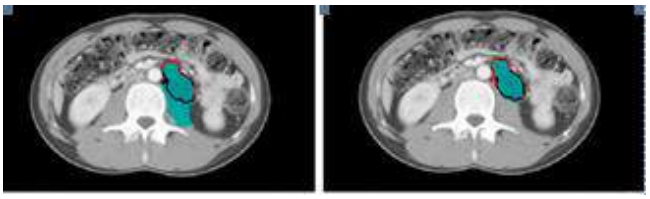

***Figura 2**. Example of segmentation. Left: Result of Algorithm 1 (in blue) Right: Result of Algorithm 2 (in blue). In red, manual segmentation provided by the specialist.*

Conclusions

In this paper the comparison and validation of two algorithms for semiautomatic segmentation of retroperitoneal tumors is presented. Both algorithms are based on continuous convex relation optimization. The first one uses a two-label implementation and the second one follows a multilabel scheme. Both algorithms have been assessed using 6 real cases (200 512x512 CT slices) and compared to their manual segmentations were provided by one specialist (used as ground truth segmentations). Several parameters such as PPV, Sensitivity, Specificity, Jaccard, or DICE coefficients were computed to quantify the performance and accuracy of both algorithms. The multilabel version performs much better than the single-label version, achieving a 90% of Sensitivity, 100% of Specificity, 88% of PPV, 80% of Jaccard index and 89% of Dice index.

	Algorithm 1					Algorithm 2				
Case	Se	Sp	PPV	Jaccard	mDice	Se	Sp	PPV	Jaccard	mDice
1	0	0	0	0	0	0,96	0,99	0,81	0,78	0,88
2	0,86	0,99	0,90	0,79	0,88	0,96	0,99	0,93	0,89	0,94
3	0,74	0,99	0,88	0,68	0,80	0,86	1	0,89	0,77	0,87
4	0,95	0,99	0,62	0,59	0,74	0,78	1	0,87	0,69	0,81
5	0,97	0,99	0,63	0,62	0,76	0,94	1	0,92	0,87	0,93
6	0,003	0,99	0	0,002	0,005	0,93	1	0,87	0,82	0,90
Mean±Desviation	0,59±0,46	0,83±0.40	0,51±0,41	0,45±0,35	0,53±0,41	0,91±0,07	1±0,01	0,88±0,04	0,80±0,07	0,89±0,05

***Table 1** Performance of Algorithm 1 and Algorithm 2*

Acknowledgments

This research has been cofinanced by P11-TIC-7727 (Government of Andalusia, Spain), PT13/0006/0036.

References

[1] Luo Z. Segmentation of liver tumor with local C-V level set. *Mechanic Automation and Control Engineering (MACE) IEEE* 2011, pp 7660-7663.

[2] Wook-Jin C, Tae-Sun C. Automated pulmonary nodule detection based on three-dimensional shape-based feature descriptor. *Comput Meth Prog Bio* 113 vol 1, 2014, pp 37-54.

[3] Kuruvilla J, Gunavathi K. Lung cancer classification using neural networks for CT images. *Comput Meth Prog Bio 113*, vol 1, 2014, pp 202-209.

[4] Sun T, Wang J, Li X, Lv P et al. Comparative evaluation of support vector machines for computer aided diagnosis of lung cancer in CT based on a multi-dimensional data set. *Comput Meth Prog Bio* vol. 111, sup 2, 2013, pp 519-524.

[5] Gao Y, et al. Prostate segmentation by sparse representation based classification. *Med Image Computing and Computer-Assisted Intervention* vol 15, 2013, pp 451-458.

[6] Moradi M, Janoos, et al. Two solutions for registration of ultrasound to MRI for image-guided prostate interventions. *Annual International Conference of the IEEE Engineering in Medicine and Biology Society, EMBS, 2012, pp.* 1129-1132.

[7] Plajer I, Nguyen-Pham T-K, Detlef Richter. Tumour Segmentation by Active Contours in 3d CT Wavelet Enhanced Image Data, *17th European Signal Processing Conference*, Glasgow, Scotland, 2009.

[8] Chen Q, Quan F, Xu J, Rubin D L. Snake model-based lymphoma segmentation for sequential CT images. *Comput Meth Prog Bio* vol. 111, sup. 2, 2013, pp 366-375.

[9] Barbu A, Suehling M, Xun X et al. Automatic Detection and Segmentation of lymph Nodes from CT Data. *IEEE T Med Imaging*, vol 31, 2012, pp 241-250.

[10] Boykov Y, Funka G. Graph cuts and efficient N-D image segmentation. *Int. J. Comput. Vision*, vol.70,2009,pp109-131.

[11] Boykov Y, Kolmogorov V. An experimental comparison of min-cut/max-flow algorithms for energy minimization in vision. *IEEE Trans. Pattern Anal. Mach. Intell*. Vol 26, 2004, pp 1124-1137.

[12] Ballangan C, et al. Lung tumor segmentation in PET images using graph cuts. *Comput Meth Prog Bio* vol.109, sup.3, 2013, pp 260-268

[13] Song Q, Chen M, Bai J et al Surface region context in optimal multi-objet Graph Based Segmentation: Robust Delineation of Pulmonary Tumors, *IPMI*, 2011, pp 61-72.

[14] Lermé N, Malgouyres F, Rocchisani JM Fast and memory efficient segmentation of lung tumors using graph cuts. *MICCAI, Third International workshop on Pulmonary Image Analysis*, Beijing, 2010, pp. 9-20.

[15] Chen V, Ryan S. Graph cut segmentation technique for MRI brain tumor extraction, *Image Processing Theory, Tool and Applications* 2010, pp 284-287.

[16] Moschidis E Graham J. Interactive Differential Segmentation of the Prostate using Graph-Cuts with a Feature Detector-based Boundary Term. *In Proc. MIUA*, 2010, pp. 191-195.

[17] Zhang J, Wang Y, Shi X. An improved graph cut segmentation method for cervical lymph nodes on sonograms and its relationship with node's shape assessment. *Comput Med Imag Grap* vol 33, 2009, pp 602-607.

[18] Suzuki K. Segmentation based features for lymph node detection from 3D Chest CT, LNC, *Machine Learning in Medical Imaging*, 7009, 2011, pp 91-99.

[19] Feulner J, Zhou S, Hammon M et al Lymph node detection and segmentation in chest CT data using discriminative learning and a spatial prior. Med Image Anal, 2012

[20] Rajiah P, et al. Imaging of Uncommon Retroperitoneal Masses. *RadioGraphics*, vol. 31, 2011, pp 049-976.

[21] Yuan J, Bae E et. al A study on continuous max-flow and min-cut approaches. *Computer Vision and Pattern Recognition*, San Francisco2010, pp 2217-2224.

[22] Bae E, et al. Global minimization for continuous multiphase partitioning problems using a dual approach. *Int. J. Comput. Vis.* Vol 92, sup1, 201, pp 112–129.

[23] Cremers D et al, Convex relaxation techniques for segmentation, stereo and multiview reconstruction. *Markov Random Fields for Vision and Image Processing* 2011.

[24] Punithakumar K, Yuan J, et al A Convex Max-Flow Approach to Distribution-Based Figure-Ground Separation, SIAM J. *Imaging Sciences* vol 5 sup 4, 2012, pp 1333-1354.

[25] Yuan J, Ukwatta E,et al A fast global optimization-based approach to evolving contours with generic shape prior. *UCLA Tech. Report CAM*, 2012, pp 12-38.

[26] Ukwatta E, Yuan J, et al. 3-D carotid multi-region MRI segmentation by globally optimal evolution of coupled surfaces. *IEEE T Med Imaging* vol32 sup4, 2013, pp770-785.

[27] Rajchl M, et al. Interactive Hierarchical Max-Flow Segmentation of Scar Tissue from Late-Enhancement Cardiac MR Images. IEEE TMI vol33 sup1, 2014, pp159-72.

[28] Ukwatta E, et al. Joint segmentation of 3D femoral lumen and outer wall surfaces from MR images, *International Conference on Medical Image Computing and Computer-Assisted Intervention*, vol 8149 2013, pp 534-541.

[29] Qiu W, Yuan J, et al. Lateral ventricle segmentation of 3D pre-term neonates US using convex optimization. *MICCAI vol 16*, 2013, pp 559-566.

[30] Yuan J, Qiu W, et al. Efficient 3D Endfiring TRUS Prostate Segmentation with Globally Optimized Rotational Symmetry. *CVPR, Conference on IEEE* 2013, pp 2211-2218.

[31] Qiu W, Yuan J et al. Prostate Segmentation: An Efficient Convex Optimization Approach With Axial Symmetry Using 3-D TRUS and MR Images. *IEEE T Med Imaging* vol 33, sup 4, 2014, pp 947-960.

[32] Perez-Carrasco J, et al Segmentation of Retroperitoneal Tumors Using Fast Continuous Max-Flow Algorithm. XIII *MEDICOM* vol 41, 2013, pp360-363.

[33] Vincent L Minimal path algorithms for the robust detection of linear features in gray images, *ISSM Proc*., Amsterdam, The Netherlands, 1998 pp. 331–338.